

Analyzing the Cross-Sensor Portability of Neural Network Architectures for LiDAR-based Semantic Labeling

Florian Piewak^{1,2}, Peter Pinggera¹, and Marius Zöllner^{2,3}

Abstract—State-of-the-art approaches for the semantic labeling of LiDAR point clouds heavily rely on the use of deep Convolutional Neural Networks (CNNs). However, transferring network architectures across different LiDAR sensor types represents a significant challenge, especially due to sensor specific design choices with regard to network architecture as well as data representation. In this paper we propose a new CNN architecture for the point-wise semantic labeling of LiDAR data which achieves state-of-the-art results while increasing portability across sensor types. This represents a significant advantage given the fast-paced development of LiDAR hardware technology. We perform a thorough quantitative cross-sensor analysis of semantic labeling performance in comparison to a state-of-the-art reference method. Our evaluation shows that the proposed architecture is indeed highly portable, yielding an improvement of 10 percentage points in the Intersection-over-Union (IoU) score when compared to the reference approach. Further, the results indicate that the proposed network architecture can provide an efficient way for the automated generation of large-scale training data for novel LiDAR sensor types without the need for extensive manual annotation or multi-modal label transfer.

I. INTRODUCTION

Within the field of autonomous driving, vehicles employ multiple sensor modalities such as cameras, RaDAR, and LiDAR to reliably perceive the environment even in challenging scenarios and adverse environmental conditions [1], [2], [3], [4]. Each sensor modality has to exploit its specific strengths in order to contribute to the overall geometric and semantic understanding of the scene. The extracted information is then combined into a holistic representation of the environment, for example an occupancy grid map [5]. This environmental representation provides the basis for high-level tasks such as localization [6], situation analysis [7] or path planning [8].

A key capability to obtain an accurate semantic understanding of an observed scene is the semantic segmentation of the sensor information. For each sensor measurement a semantic class is inferred, yielding a fine-grained prediction of the observed obstacle types (see Fig. 1 and Fig. 2) The individual predictions can then be combined into a compact object-level representation [9].

The task of semantic segmentation or semantic labeling originated in the field of computer vision, with the aim to individually classify each pixel in a given image [10]. Within recent years, this task has been applied successfully to other

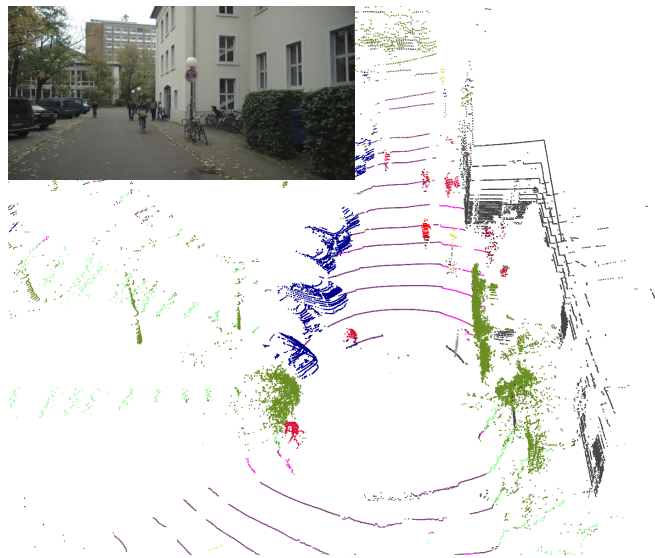


Fig. 1. Exemplary semantic labeling result obtained via the proposed *PiLaNet* on a VLP-32C point cloud. The corresponding camera image on the top left is shown for clarity, with the camera’s field of view covering the top center of the point cloud. The following semantic classes are visualized: road, sidewalk, person, rider, small vehicle, large vehicle, two wheeler, construction, pole, traffic sign, vegetation, terrain.

sensor modalities such as LiDAR or RaDAR [11]. Across all modalities state-of-the-art results are obtained by modern deep learning techniques. However, approaches based on the application of deep Convolutional Neural Networks (CNNs) are often tailored to the specific characteristics of the respective sensor instance. Transferring a network architecture from e.g. one LiDAR sensor model to another represents a significant challenge, especially due to sensor specific design choices with regard to network architecture as well as data representation. This effect is intensified by the fact that LiDAR sensor technology keeps evolving at a fast pace, with numerous new sensor types being announced or released to the market every year, featuring novel scanning patterns and ever increasing range and spatial resolution.

When training deep neural networks, large scale datasets are required in order to obtain state-of-the-art results. Generating manually annotated point cloud data for LiDAR-based semantic labeling at scale presents a vast effort and involves even higher cost than manual image annotation in the computer vision domain. This is due to the additional spatial dimension as well as the sparsity of the data, which yields a representation that is non-intuitive and tedious for human annotators. Therefore, some authors have used

¹Daimler AG, R&D, Stuttgart, Germany

²Karlsruhe Institute of Technology, Karlsruhe, Germany

³FZI Research Center for Information Technology, Karlsruhe, Germany
Primary contact: florian.piewak@daimler.com

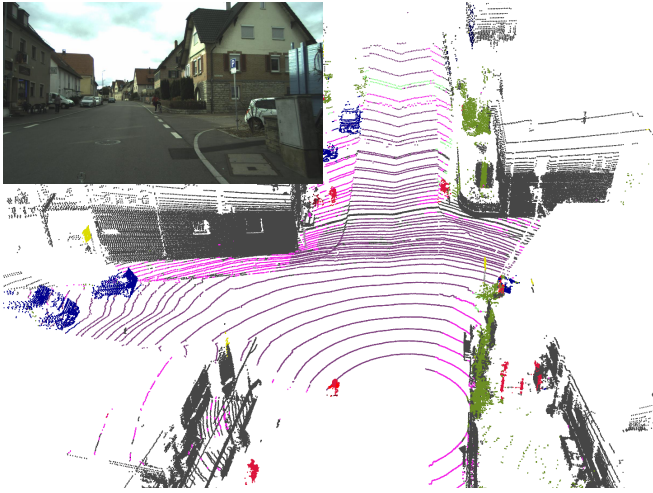


Fig. 2. Exemplary semantic labeling result obtained via the proposed *PiLaNet* on a VLS-128 point cloud. The corresponding camera image on the top left is shown for clarity, with the camera’s field of view covering the top center of the point cloud. The following semantic classes are visualized: road, sidewalk, person, rider, small vehicle, large vehicle, two wheeler, construction, pole, traffic sign, vegetation, terrain.

existing datasets dedicated to other tasks such as 3D object detection [12] to extract point-wise LiDAR semantics [13], [14]. However, only a small number of semantic classes can be extracted in this way. An alternative approach to generate 3D training data is based on the transfer of semantic information from a registered camera image to the LiDAR domain [15], [16]. While this allows the automated generation of large amounts of training data, the quality of the result strongly depends on the accuracy of the image-based semantics, the extrinsic and intrinsic calibration as well as the temporal synchronization of the different sensor modalities.

Given the sensor specific tailoring of many current CNN architectures as well as the difficulty of generating annotated training data at scale, in this paper we consider the cross-sensor portability of neural network architectures for LiDAR-based semantic labeling. Portable network architectures could provide a solution to above challenges by enabling the reuse of annotated data and reducing the effort required for adapting CNN architectures to new sensor models.

Our main contributions can be summarized as follows:

- 1) We present a portable Convolutional Neural Network (CNN) architecture for high-quality semantic labeling of semi-dense point clouds across different sensor models.
- 2) We perform a thorough quantitative cross-sensor evaluation of the semantic labeling performance in comparison to state-of-the-art approaches. Our experimental analysis is based on extensive dedicated datasets from two state-of-the-art LiDAR sensors with strongly differing spatial resolution.

II. RELATED WORK

In recent years LiDAR point cloud processing has gained more and more attention due to decreasing hardware costs and an increasing number of sensor makes and models available on the market. The main difference between the different algorithmic approaches is the representation of the 3D point cloud to be processed. Three different types of point cloud representations are commonly found in the literature:

First, the point cloud can be represented as a projection of the 3D data to 2D space. For example Yang et al. [17] and Beltrán et al. [18] use a bird’s eye view (BEV) to extract bounding boxes for different types of objects from the KITTI dataset [12]. Other approaches use a cylindrical projection of the LiDAR point cloud, e.g. for semantic segmentation [14], [19], [13], [16], [20]. In contrast to other projection methods such as the bird’s eye view, the cylindrical projection provides a lossless transformation of the input data. The main advantage of the described projection methods is the efficient processing based on 2D convolutions. However, the generated CNNs are usually rather sensor specific and can only be transferred to different sensor models with significant effort.

An alternative method to represent point clouds is by way of an unordered point set [21], [22], [23]. Qi et al. [21] propose the so-called PointNet, which first processes each point independently and then extracts global features using a max pooling operator. Based on that global feature a classification of the point cloud can be obtained. While this approach is able to handle an arbitrary number of unordered points, the resulting performance tend to be problematic in large-scale outdoor scenarios as are usually encountered in the field of autonomous driving.

The third common type of point cloud representation performs a discretization of the 3D space into a voxel grid [24] or an octree [25]. Rieger et al. [25] evaluate a semantic segmentation task by predicting a single semantic class for all points within an octree cell. Occupancy information is used as a feature for each voxel. Zhou et al. propose VoxelNet [26] for the task of object detection. Here the idea of PointNet [21] is adopted to extract features from an arbitrary number of points per voxel. While this representation increases cross-sensor portability due to the regularity of the voxel grid, the additional dimension and the employed 3D convolutions drastically increase the training and inference times for larger CNN architectures. Lang et al. alleviate this problem by introducing PointPillars [27]. Here the 3D space is compressed to 2.5D by reducing the number of voxels along the vertical axis to one, leading to an intermediate structure resembling pillars. Similar to BEV-based approaches, this 2.5D pseudo-image can then be processed using 2D convolutions, thereby benefiting from the learned features per pillar. Both VoxelNet [26] and PointPillars [27] are optimized for object detection tasks. In this paper we build upon these approaches and propose a CNN architecture for point-wise semantic segmentation which is portable across different LiDAR sensors.

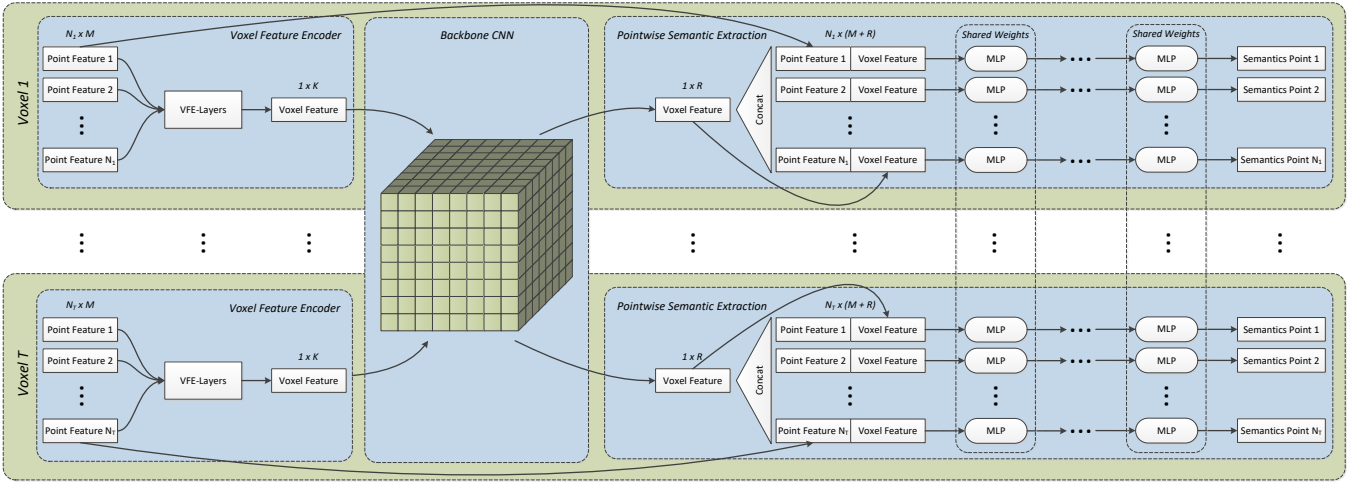


Fig. 3. 3D voxel CNN architecture for point-wise semantic segmentation. The voxel space as well the processing chain per voxel are represented in green. The three main components (voxel feature encoder, backbone CNN, and point-wise semantic extraction head) are represented as blue boxes.

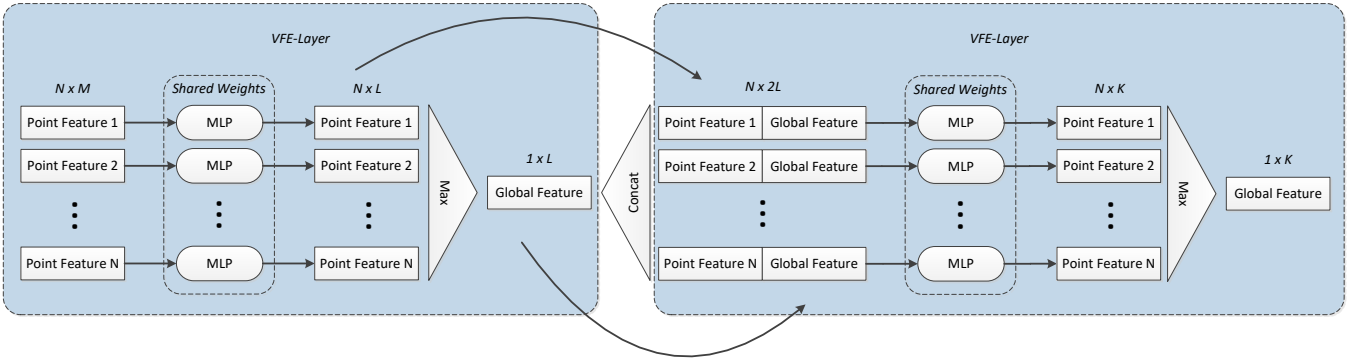


Fig. 4. Example of a voxel feature encoder based on two consecutive VFE-Layers. The original point features serve as input to the first VFE-Layer, while the second VFE-Layer uses the combination of the point-wise features with the global features as input.

III. METHOD

In this paper, we extend previous work and propose a new CNN architecture for the point-wise semantic labeling of LiDAR data. The presented architecture achieves state-of-the-art results while increasing portability across sensor types at the same time. We choose a voxel-based processing approach, similar to the data structures used by VoxelNet [26] and PointPillars [27]. Hence, the resulting pillar-based labeling network is called *PiLaNet*. Within the following subsections, the network architecture is described in detail. It consists of three main components (see Fig. 3):

- the Voxel Feature Encoder (VFE), which generates a feature vector that encodes the properties of the voxel content,
- the backbone CNN, which accumulates the generated voxel features in 3D space and
- the point-wise semantic extraction head, which infers a semantic label for each point from the encoded voxel features.

A. Voxel Feature Encoder

The voxel feature encoder¹ represents a network component designed to condense the essential properties of all points contained within a voxel into one feature vector (see Fig. 4). This idea was originally proposed in PointNet [21] to encode a full point cloud into a single feature vector. It was later adapted and applied to individual voxels in the VoxelNet architecture [26]. Each point is represented by its global cartesian coordinates x_g , y_g and z_g , the measured reflectivity r as well as the relative cartesian coordinates with respect to the mean of all points within a voxel x_v , y_v and z_v . To obtain an initial point-wise feature encoding, each point is processed individually via multi layer perceptrons (MLP). These sub-networks use shared weights to enforce identical feature encoders for each point. Subsequently a max pooling operator is applied to the point-wise features in order to generate a single feature vector per voxel. The combination of these processing steps is also known as VFE-Layer in the literature [26].

The VFE-Layer can be applied repeatedly by concatenating the encoded point-wise features with the voxel feature

¹also called voxel feature extractor

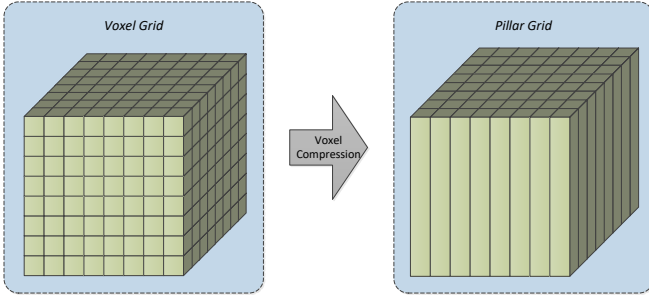


Fig. 5. Compression of the 3D space to 2.5D by reducing the number of voxels along the vertical axis to one, leading to an intermediate structure resembling pillars as proposed in [27].

vector resulting from the previous step (see Fig. 4). Eventually the MLPs as well as the max pooling operator are applied once more to obtain a final refined feature vector for each voxel.

Since the voxel feature encoder can handle arbitrary numbers of input points, it is applicable to various voxel sizes and point cloud densities. It provides a parameterizable representation which is highly portable between different sensor types.

The features computed by the VFE-Layers are combined into a 3D voxel grid which forms the input to the backbone CNN described in the next subsection.

B. Backbone CNN

To fully exploit the spatial context within the encoded data, a CNN backbone architecture is applied to the voxel grid. Here, various architectural choices are possible. VoxelNet [26] employs a full 3D backbone CNN to extract features from the voxel representation via 3D convolutions. This architecture is well suited for the task of object detection, where the size of the 3D representation can be reduced by applying pooling layers or strided convolutions without a significant loss in output accuracy. However, for the semantic segmentation task considered in this paper a fine-grained point-wise prediction is required. In this case a full 3D CNN entails high computational complexity leading to excessive memory consumption as well as long training and inference times. To reduce the dimensionality of the voxel grid and hence the computational complexity of the backbone CNN, we adopt the concept of pillars as proposed in [27] (see Fig. 5). The dimensionality of the voxel grid is reduced by directly encoding the height information of each point within its associated pillar. The resulting representation resembles a two-dimensional pseudo-image, similar to a bird’s eye view. Consequently, a 2D CNN architecture can be applied to process the voxel representation in an efficient way while retaining the full information of the encoded data.

C. Point-Wise Semantic Extraction

The backbone CNN yields voxel-wise output features, similar to the probability score maps of object detection approaches [26], [27]. These features can be used to infer a semantic class for each voxel. However, to obtain a

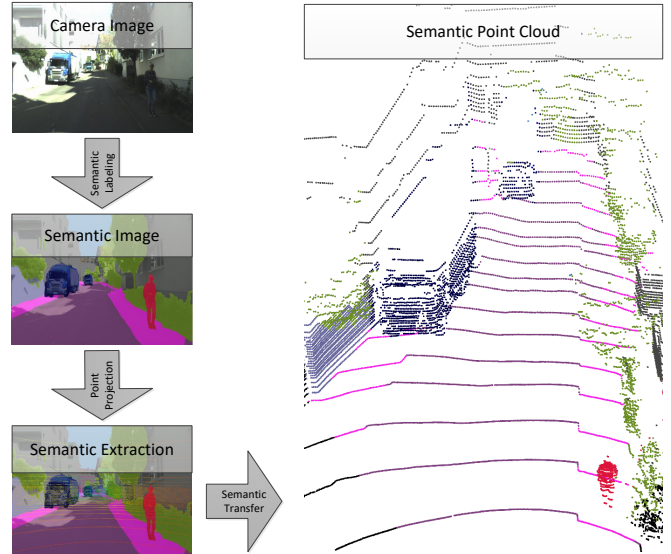


Fig. 6. Illustration of the *Autolabeling* method of [16] used to transfer semantic reference data from a camera image to a point cloud (VLP-32C).

point-wise semantic segmentation result this approach is not sufficient, especially for large voxels such as pillars where all points within a voxel would be assigned the same semantic class. Therefore, we introduce a point-wise semantic extraction head as shown in Fig. 3. For each point, the corresponding output vector $(x_g, y_g, z_g, r, x_v, y_v, z_v)$ of the voxel feature encoder is concatenated with the voxel-wise features extracted by the backbone CNN. Subsequently, each point is processed independently by multiple MLPs to extract a point-wise classification result independent of its containing voxel. In this way fine-grained semantic class predictions within one voxel are achieved.

IV. DATASET

In the following analysis of the cross-sensor portability of different network architectures, we employ extensive dedicated datasets based on two state-of-the-art LiDAR sensors: a Velodyne VLP-32C and a Velodyne VLS-128. The VLP-32C dataset consists of point clouds with 32 layers (rows) and is the same dataset as used in [16] (see Table I). The ground truth data is generated in two different ways: First, the full dataset is semantically annotated in an automated way using the *Autolabeling* method proposed in [16] (see Fig. 6). Here, a dedicated CNN is used to process a registered RGB camera image. This CNN is trained on the Cityscapes [28] dataset to obtain a high-quality semantic segmentation result. The LiDAR point-cloud is then projected into the camera image and the semantic labels of the image are transferred to the individual points. Second, a small number of point clouds is manually annotated in order to both fine-tune and evaluate the analyzed CNN architectures. The overall dataset is split into three subsets. One subset for training the networks (*training*), one subset for validation as well as optimization of the hyper-parameters of the architectures (*validation*), and one subset for the final evaluation (*testing*).

TABLE I

SPLIT OF THE TWO EMPLOYED DATASETS INTO THE SUBSETS FOR TRAINING, VALIDATION AND TESTING. WE DISTINGUISH BETWEEN AUTOMATICALLY AND MANUALLY ANNOTATED POINT CLOUDS (FRAMES).

	Training	Validation	Testing
Autolabeled Frames VLP-32C	344,027	73,487	137,682
Autolabeled Frames VLS-128	179,042	31,139	84,839
Man. Annotated Frames VLP-32C	1,909	373	718
Man. Annotated Frames VLS-128	1,257	335	1,110

The dataset based on the Velodyne VLS-128, a LiDAR with 128 layers, is generated in a similar way. It includes various scenarios such as highways, rural roads, and urban traffic. The data is also split into three subsets for training, optimizing hyper-parameters and the final evaluation. Similar to the VLP-32C dataset, the ground truth is generated in two ways. The full dataset is annotated automatically via the *Autolabeling* method, while a small number of frames is manually annotated. We note that the VLS-128 dataset is approximately half the size of the VLP-32C dataset (see Table I).

For both datasets the set of semantic classes is identical to the one defined in [16]. It consists of the following twelve classes: road, sidewalk, person, rider, small vehicle, large vehicle, two-wheeler, construction, pole, traffic sign, vegetation, and terrain (see Fig. 1 and Fig. 2).

V. EXPERIMENTS

In this chapter the proposed network architecture *PiLaNet* is evaluated against a state-of-the-art reference method, with a focus on cross-sensor portability. We use the 2D CNN architecture called *LiLaNet* of Piewak et al. [16] as our reference.

PiLaNet implements the voxel representation as described in Section III, where we limit the voxel space to the range $(0.0m, -30.0m, -2.0m) \leq (x_g, y_g, z_g) \leq (60.0m, 30.0m, 9.2m)$. The number of voxels is set to $(num_x, num_y, num_z) = (300, 300, 1)$. These parameters were optimized based on available GPU memory, overall network performance, and training time. The used voxel feature encoder is composed of two VFE-Layers as described in Section III-A, with a voxel feature vector size of 128. For the implementation of the VFE, we restrict the maximum number of points per voxel to 35 and apply random sampling in case the limit is exceeded. Since we use a single voxel along the z axis (pillars), the backbone is modeled as a 2D CNN. For a valid comparison to the reference approach, we use the same architecture for the backbone CNN as used for *LiLaNet* [16], with the number of output features per voxel set to 24. The point-wise semantic extraction head includes three consecutive MLP layers with 64, 64, and 12 features. The last layer provides the scores of the 12 semantic classes. Aside from the classification score, after each layer a rectified linear unit (ReLU) is applied.

Note that we do not optimize either of the considered

networks architectures for the specific sensor types. In this way we achieve a valid evaluation of the unmodified CNN architectures and corresponding point-cloud representations in terms of cross-sensor portability.

The training of both *LiLaNet* and *PiLaNet* is performed with a batch size² $b = 8$ via the Adam solver [29]. With regard to training strategy, we follow the suggestion of [16] and first train on the autolabeled training subset, followed by a fine-tuning step on the manually annotated training subset. The training on the autolabeled set is run for 300,000 iterations before starting the fine-tuning. As training parameters we use the suggested default values for the Adam solver of $\beta_1 = 0.9$, $\beta_2 = 0.999$ and $\epsilon = 10^{-8}$. The learning rate is fixed at $\alpha = 10^{-3}$ ($\alpha = 10^{-4}$ for fine-tuning), while the weights are initialized with MSRA [30].

Evaluation is performed based on the testing subset of the manually annotated frames, where for each class the Intersection over Union (IoU) metric as well as the overall mean IoU is calculated. We restrict the evaluation to the defined voxel range to ensure comparability between the different point cloud representations, i.e. the voxel representation used by *PiLaNet* and the cylindrical 2D projection of *LiLaNet*.

Several evaluation stages are performed on both datasets, which we discuss in more detail in the following subsections:

- 1) Quality of the *Autolabeling* result
- 2) Performance of the networks (*LiLaNet* and *PiLaNet*) trained, fine-tuned, and evaluated on the same sensor
- 3) Performance of the networks (*LiLaNet* and *PiLaNet*) trained and fine-tuned on one sensor and evaluated on the other sensor
- 4) Performance of the networks (*LiLaNet* and *PiLaNet*) trained and fine-tuned on one sensor and additionally fine-tuned as well as evaluated on the other sensor

A. Autolabeling Quality

The quality of the point cloud semantics obtained by the *Autolabeling* method is summarized in the first two rows of Table II³. These values provide a reference which the CNN can be expected to reach without fine-tuning on manually annotated data. It has to be noted that the results on the VLP-32C dataset are slightly better than on the VLS-128 dataset. This is due to differences in the recording setup, including extrinsic calibration data. The lower resolution of the VLP-32C makes the process less susceptible to errors caused by calibration inaccuracies. Nevertheless, the results lie within a similar range and allow for an initial assessment of the quality of the datasets.

B. Same-Sensor Evaluation

First, the networks are trained as described in Section V, where training, fine-tuning as well as evaluation is performed on the same dataset, but on different subsets. The second

²In case the network does not fit into GPU memory, the batch is distributed over multiple devices.

³The *Autolabeling* results differ from the values reported in [16] due to the restriction to the voxel range.

TABLE II

OVERVIEW OF THE RESULTS OBTAINED IN THE DIFFERENT EVALUATION STAGES DESCRIBED IN SECTION V. EACH ROW REPRESENTS A SEMANTIC SEGMENTATION APPROACH. THE CORRESPONDING DESCRIPTIONS ARE GIVEN IN THE FIRST COLUMN, WHERE THE FIRST TWO ROWS DESCRIBE THE ARCHITECTURE AND THE TRAINING DATASET AS WELL THE ADDITIONAL FINE-TUNING DATASET (IF USED). THE LAST ROW OF THE DESCRIPTION DENOTES THE DATASET USED FOR EVALUATION. THE TOP RESULTS OF THE RESPECTIVE NETWORK ARCHITECTURES TRAINED WITH THE SAME STRATEGY ARE MARKED IN BOLD.

	road	sidewalk	person	rider	small vehicle	large vehicle	two wheeler	construction	pole	traffic sign	vegetation	terrain	mean IoU
<i>Autolabeling</i> evaluation VLP-32C	90.3%	62.4%	79.7%	52.7%	83.1%	61.9%	46.5%	76.5%	33.6%	45.1%	79.6%	55.5%	63.9%
<i>Autolabeling</i> evaluation VLS-128	88.3%	58.3%	64.2%	44.6%	82.8%	56.6%	39.8%	83.0%	26.5%	36.7%	83.1%	55.4%	60.1%
<i>LiLaNet</i> VLP-32C evaluation VLP-32C	93.9%	73.0%	72.2%	45.3%	86.3%	49.3%	47.2%	84.1%	48.3%	79.0%	83.0%	66.6%	69.0%
<i>PiLaNet</i> VLP-32C evaluation VLP-32C	93.2%	69.8%	81.8%	50.2%	88.9%	67.3%	47.5%	81.6%	48.8%	77.5%	79.4%	64.3%	70.9%
<i>LiLaNet</i> VLS-128 evaluation VLS-128	89.9%	62.3%	59.5%	19.1%	82.1%	24.8%	31.5%	83.5%	41.3%	48.3%	85.0%	65.7%	57.7%
<i>PiLaNet</i> VLS-128 evaluation VLS-128	91.1%	63.9%	69.1%	49.7%	88.5%	41.9%	40.0%	85.3%	47.4%	42.2%	84.5%	64.2%	64.0%
<i>LiLaNet</i> VLP-32C evaluation VLS-128	55.6%	19.9%	17.5%	7.5%	45.1%	4.6%	9.5%	65.7%	33.4%	36.5%	72.7%	28.0%	33.0%
<i>PiLaNet</i> VLP-32C evaluation VLS-128	46.5%	20.0%	48.5%	35.4%	81.2%	34.5%	20.3%	73.7%	41.3%	33.9%	77.1%	30.7%	45.2%
<i>LiLaNet</i> VLS-128 evaluation VLP-32C	83.0%	30.8%	40.2%	4.8%	68.3%	22.7%	19.5%	63.8%	29.6%	46.3%	68.1%	49.7%	43.9%
<i>PiLaNet</i> VLS-128 evaluation VLP-32C	86.2%	50.4%	75.9%	36.5%	80.8%	34.0%	28.4%	69.5%	35.4%	35.5%	70.5%	47.5%	54.2%
<i>LiLaNet</i> VLP-32C finetuned VLS-128 evaluation VLS-128	87.8%	58.0%	46.0%	13.6%	77.1%	14.1%	25.0%	81.5%	39.0%	46.0%	84.4%	65.2%	53.2%
<i>PiLaNet</i> VLP-32C finetuned VLS-128 evaluation VLS-128	88.5%	58.0%	64.9%	42.5%	87.3%	49.5%	36.9%	84.4%	45.6%	45.1%	83.6%	63.1%	62.5%
<i>LiLaNet</i> VLS-128 finetuned VLP-32C evaluation VLP-32C	92.2%	66.3%	63.8%	29.1%	83.1%	45.6%	36.5%	80.3%	41.1%	75.8%	80.1%	63.8%	63.1%
<i>PiLaNet</i> VLS-128 finetuned VLP-32C evaluation VLP-32C	92.6%	66.6%	77.6%	53.1%	86.8%	58.8%	39.0%	78.9%	43.6%	76.3%	77.3%	62.3%	67.7%

block of Table II shows the results of this same-sensor evaluation strategy. The proposed *PiLaNet* clearly outperforms *LiLaNet* on the VLS-128 dataset and reaches slightly better results on the VLS-32C dataset as well. This indicates that the voxel representation outperforms the cylindrical 2D representation in terms of output quality. However, compared to *LiLaNet*, the inference time of *PiLaNet* increases by a factor of 7 for the VLP-32C and a factor of 2 for the VLS-128. This is mainly caused by the required voxelization and the larger dimensions of the backbone CNN input pseudo-image.

Interestingly, both network architectures achieve better results on the VLP-32C dataset than on the VLS-128 dataset. This effect is mainly due to the smaller overall size of the VLS-128 dataset. Also, the decrease in performance is larger for *LiLaNet* than for *PiLaNet*. This can be attributed to the higher resolution of the VLS-128, which directly influences the object sizes within the cylindrical point cloud

representation. This indicates that the *PiLaNet* architecture is more suitable for transfer between sensors than *LiLaNet*.

C. Cross-Sensor Evaluation

Using the already trained networks of Section V-B, the second evaluation stage is performed on the data of the opposite sensor in order to evaluate cross-sensor portability. The corresponding results are listed in the third block of Table II. *PiLaNet* clearly outperforms *LiLaNet* by more than 10 percentage points, confirming that the voxel representation results in a far more portable architecture than the cylindrical projection. At the same time the mean IoU of *PiLaNet* drops by more than 16 percentage points compared to the same-sensor evaluation results. This drop might in part be due to the backbone CNN, which has to handle strongly varying densities for the different sensor types and resolutions. While the cross-sensor results are very promising, we note that there is still ample room for tuning the voxel representation for portability.

D. Cross-Sensor Finetuning

As seen in Section V-C, the direct application of network models to different sensors leads to a significant drop in the output performance. Therefore, we propose a data-driven adaptation step where the pre-trained model is fine-tuned on the target sensor using manually annotated data. Note that only a small amount of manually annotated data is required, while the full amount of autolabeled data of the target sensor is not used. The results of this strategy are shown in the fourth block of Table II. After fine-tuning the network architecture on the target sensor, *PiLaNet* still outperforms *LiLaNet*, which once more confirms the superior portability of the *PiLaNet* architecture, allowing for an adaptation to the target sensor type with only small amounts of additional data.

When compared to pure *Autolabeling* this training strategy increases the mean IoU of *PiLaNet* by 2.4 percentage points on the VLS-128 dataset and by 3.8 percentage points on the VLP-32C data. This shows that the presented adaptation process can be used to successfully transfer network architectures across sensors by applying only a small manually annotated dataset for fine-tuning instead of using another sensor modality such as cameras to generate reference data. It is conceivable that a fine-tuned *PiLaNet* can be used to extend the *Autolabeling* concept of [16], which originally relies on an additional sensor modality, in order to automatically generate large-scale datasets for new sensor types of the same modality (e.g. LiDAR to LiDAR *Autolabeling*).

VI. CONCLUSION

In this paper, we present a CNN architecture for the fine-grained semantic segmentation of LiDAR point clouds based on a pillar-like voxel representation. The proposed architecture is designed for portability across different LiDAR sensor types to successfully handle varying spatial resolution and scanning patterns. We evaluate the network architecture against a state-of-the-art semantic segmentation approach based on a cylindrical projection of the LiDAR data [16]. Our evaluation on manually annotated data across different sensors shows that the proposed architecture is indeed highly portable, yielding an improvement of 10 percentage points in IoU when compared to the reference approach of [16]. However, the employed voxel representation leads to an increase in computational complexity, resulting in significantly longer inference times.

We further show that the presented architecture can be fully transferred across different sensor types with minimal adaptation effort by fine-tuning the pre-trained network on a small target sensor dataset. This represents a significant advantage given the fast-paced development of LiDAR hardware technology. The results indicate that the proposed network architecture can provide an efficient way for the automated generation of large-scale training data for novel LiDAR sensor types without the need for a multi-modal sensor setup. Hence, it might complement or even replace the multi-modal *Autolabeling* method of [16].

Additional measures to further increase the cross-sensor portability of the considered methods include the optimization of the voxel layout and the backbone CNN architecture as well as classical data augmentation methods.

REFERENCES

- [1] M. Aeberhard, S. Rauch, M. Bahram, G. Tanzmeister, J. Thomas, Y. Pilat, F. Himm, W. Huber, and N. Kaempchen, "Experience, results and lessons learned from automated driving on Germany's highways," *Intelligent Transportation Systems Magazine*, vol. 7, no. 1, pp. 42–57, 2015.
- [2] J. Ziegler, P. Bender, M. Schreiber, and Others, "Making Bertha Drive - An Autonomous Journey on a Historic Route," *Intelligent Transportation Systems Magazine*, vol. 6, no. 2, pp. 8–20, 2014.
- [3] C. Urmsion, C. Baker, J. Dolan, and Others, "Autonomous Driving in Traffic: Boss and the Urban Challenge," *AI Magazine*, vol. 30, no. 2, pp. 17–28, 2009.
- [4] S. Thrun, M. Montemerlo, H. Dahlkamp, D. Stavens, A. Aron, J. Diebel, P. Fong, J. Gale, M. Halpenny, and G. Hoffmann, "Stanley, the Robot that Won the DARPA Grand Challenge," *Journal of Field Robotics*, vol. 23, no. 9, pp. 661–692, 2006.
- [5] D. Nuss, S. Reuter, M. Thom, T. Yuan, G. Krehl, M. Maile, A. Gern, and K. Dietmayer, "A random finite set approach for dynamic occupancy grid maps with real-time application," *International Journal of Robotics Research*, vol. 37, no. 8, pp. 841–866, 2018.
- [6] T.-d. Vu, J. Burlet, O. Aycard, and Others, "Grid-based localization and local mapping with moving object detection and tracking Grid-based Localization and Local Mapping with Moving Object Detection and Tracking," *Journal Information Fusion*, vol. 12, no. 1, pp. 58–69, 2011.
- [7] C. Laugier, I. E. Paromtchik, M. Perrollaz, M. Y. Yong, J.-D. Yoder, C. Tay, K. Mekhnacha, and A. Negre, "Probabilistic Analysis of Dynamic Scenes and Collision Risks Assessment to Improve Driving Safety," *Intelligent Transportation Systems Magazine (ITSM)*, vol. 3, no. 4, pp. 4–19, 2011.
- [8] H. Bai, S. Cai, N. Ye, and Others, "Intention-aware online POMDP planning for autonomous driving in a crowd," in *International Conference on Robotics and Automation (ICRA)*, 2015.
- [9] R. Barea, C. Perez, L. M. Bergasa, E. Lopez-Guillen, E. Romera, E. Molinos, M. Ocana, and J. Lopez, "Vehicle Detection and Localization using 3D LIDAR Point Cloud and Image Semantic Segmentation," *Intelligent Transportation Systems Conference (ITSC)*, 2018.
- [10] A. Garcia-Garcia, S. Orts-Escolano, S. Oprea, and Others, "A Review on Deep Learning Techniques Applied to Semantic Segmentation," in *arXiv preprint: 1704.06857*, 2017.
- [11] D. Feng, C. Haase-Schuetz, L. Rosenbaum, H. Hertlein, F. Duffhaus, C. Glaeser, W. Wiesbeck, and K. Dietmayer, "Deep Multi-modal Object Detection and Semantic Segmentation for Autonomous Driving: Datasets, Methods, and Challenges," *arXiv preprint: 1902.07830*, 2019.
- [12] A. Geiger, P. Lenz, and R. Urtasun, "Are we ready for autonomous driving? the KITTI vision benchmark suite," in *Conference on Computer Vision and Pattern Recognition (CVPR)*, 2012.
- [13] B. Wu, X. Zhou, S. Zhao, X. Yue, and K. Keutzer, "SqueezeSegV2: Improved Model Structure and Unsupervised Domain Adaptation for Road-Object Segmentation from a LiDAR Point Cloud," *arXiv preprint: 1809.08495*, 2018.
- [14] A. Dewan, G. L. Oliveira, and W. Burgard, "Deep Semantic Classification for 3D LiDAR Data," in *International Conference on Intelligent Robots and Systems (IROS)*, 2017.
- [15] R. Varga, A. Costea, H. Florea, and Others, "Super-sensor for 360-degree Environment Perception: Point Cloud Segmentation Using Image Features," in *International Conference on Intelligent Transportation Systems (ITSC)*, 2017.
- [16] F. Piewak, P. Pinggera, M. Schäfer, D. Peter, B. Schwarz, N. Schneider, M. Enzweiler, D. Pfeiffer, and M. Zöllner, "Boosting LiDAR-Based Semantic Labeling by Cross-modal Training Data Generation," in *European Conference on Computer Vision Workshops (ECCV)*, 2018.
- [17] B. Yang, W. Luo, and R. Urtasun, "PIXOR: Real-time 3D Object Detection from Point Clouds," in *Computer Vision and Pattern Recognition (CVPR)*, 2018.

- [18] J. Beltrán, C. Guindel, F. M. Moreno, D. Cruzado, F. García, and A. De La Escalera, "BirdNet: A 3D Object Detection Framework from LiDAR Information," *Intelligent Transportation Systems Conference (ITSC)*, 2018.
- [19] Y. Wang, T. Shi, P. Yun, L. Tai, and M. Liu, "PointSeg: Real-Time Semantic Segmentation Based on 3D LiDAR Point Cloud," *arXiv preprint: 1807.06288*, 2018.
- [20] J. Mei, B. Gao, D. Xu, W. Yao, X. Zhao, and H. Zhao, "Semantic Segmentation of 3D LiDAR Data in Dynamic Scene Using Semi-supervised Learning," *arXiv preprint: 1809.00426*, 2018.
- [21] C. R. Qi, H. Su, K. Mo, and Others, "PointNet: Deep Learning on Point Sets for 3D Classification and Segmentation," in *Computer Vision and Pattern Recognition (CVPR)*, 2017.
- [22] C. R. Qi, L. Yi, H. Su, and Others, "PointNet++: Deep Hierarchical Feature Learning on Point Sets in a Metric Space," in *Advances in Neural Information Processing Systems (NIPS)*, 2017.
- [23] Y. Li, R. Bu, M. Sun, and Others, "PointCNN: Convolution On X-Transformed Points," in *Advances in Neural Information Processing Systems (NIPS)*, 2018.
- [24] D. Maturana and S. Scherer, "VoxNet: A 3D Convolutional Neural Network for Real-Time Object Recognition," in *International Conference on Intelligent Robots and Systems (IROS)*, 2015.
- [25] G. Riegler, A. O. Ulusoy, and A. Geiger, "OctNet: Learning Deep 3D Representations at High Resolutions," in *Computer Vision and Pattern Recognition (CVPR)*, 2017.
- [26] Y. Zhou and O. Tuzel, "VoxelNet: End-to-End Learning for Point Cloud Based 3D Object Detection," in *Conference on Computer Vision and Pattern Recognition (CVPR)*, 2018.
- [27] A. H. Lang, S. Vora, H. Caesar, L. Zhou, J. Yang, and O. Beijbom, "PointPillars: Fast Encoders for Object Detection from Point Clouds," *arXiv preprint: 1812.05784*, 2018.
- [28] M. Cordts, M. Omran, S. Ramos, and Others, "The Cityscapes Dataset for Semantic Urban Scene Understanding," in *Conference on Computer Vision and Pattern Recognition (CVPR)*, 2016.
- [29] D. P. Kingma and J. Ba, "Adam: A Method for Stochastic Optimization," in *arXiv preprint: 1412.6980*, 2014.
- [30] K. He, X. Zhang, S. Ren, and Others, "Delving Deep into Rectifiers: Surpassing Human-Level Performance on ImageNet Classification," in *International Conference on Computer Vision (ICCV)*, 2015.